This project has received funding from the European Union's Horizon 2020 research and innovation programme under under FET-Open grant agreement no. 899646 (k-NET)

INTERNAL REPORT

Project acronym	k-NET
Project full title	k-Space Neural Computation with magnetic excitations
Grant Agreement no.	899646

Document title	Deliverable 3.2 – Report on the experimental control of the coupling coefficients between modes
Revision no.	1
Document date	25/02/2023
Dissemination level	Confidential
Responsible partner	CREATE
Contributing partners	WWU, CREATE, THALES, CNRS
Reviewing partners	All

CHANGE RECORD

Revision	Date	Changes	Authors	Status
1	24/02/2023	version 1	S. O. Demokritov V. E. Demidov H. Merbouche	Submit-ted

TABLE OF CONTENTS

SUMMARY

The ultimate goal of the k-NET project is to demonstrate the possibility of utilizing interacting spin-wave eigenmodes for the implementation of neuromorphic computation in the k-space. Within this k-space neural network (k-NN) concept, the discrete spin-wave modes in microscopic magnetic structures play the role of neurons, while the nonlinear interactions among them represent synapses (as schematically represented in Figure 1).

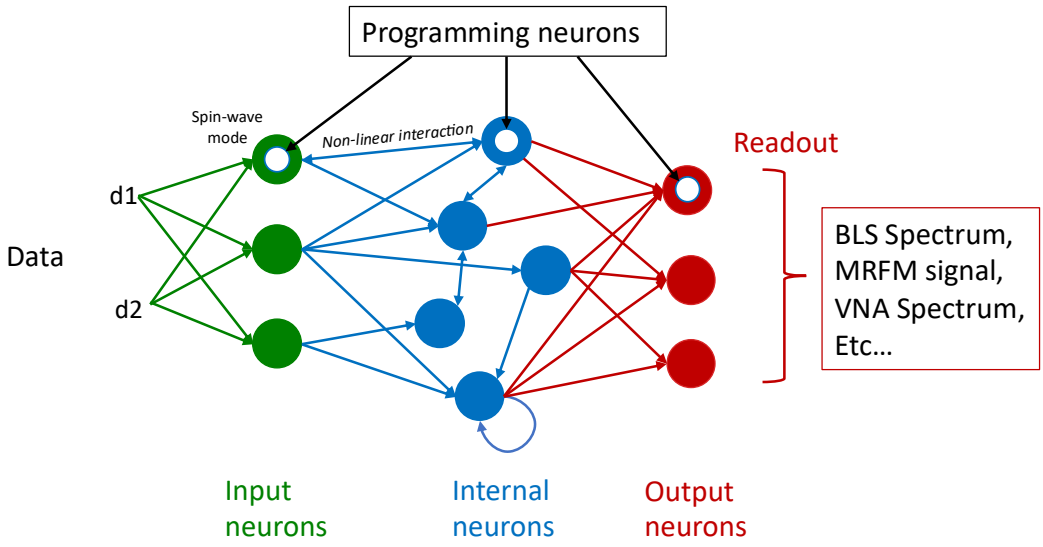

Figure 1: Schematics of a k-NN.

In all possible implementations, the neurons can be decomposed in four categories:

1. The input neurons, i.e. the modes that are directly addressed by a data-dependent signal during training and computing.
2. The programming neurons, i.e. the modes that are excited by a data-independent signal. They prepare the system to be in a state that is favorable to the computing task.
3. Internal neurons, i.e. modes that are not directly addressed, but contribute to the computation. Ideally the total number of contributing neurons should be as large as possible.
4. The output neurons, i.e. the modes that contribute to the read-out of the state of the system and eventually give the result of the computation.

In the linear regime, all the modes are independent of each other, and the neural network has zero synapse (or all synapses have a weight equal to zero). In order to create synapses we use a strong direct excitation to put the system in a non-linear state. In the first part, we describe the experimental set up and the observation of the efficient scattering of magnons from one mode to another or to multiple other detectable modes above a certain threshold, through a process which can be treated as modulation instability or four-magnon scattering.

We then use a secondary source to modulate the scattering and assess how we can experimentally control the synaptic weights in a k-space neural network. We demonstrate that the secondary source can stimulate the spontaneous scattering initiated by the primary source and that this stimulation depends on the applied frequency and power.

1 SELF MODULATION USING DIRECT EXCITATION

1.1 Experimental set-up

In the measurements described below, we used the first generation of samples prepared within WP1 of the k-NET project, which are described in detail in the technical report D1.1. The spin-wave modes were studied in microscopic disks with the diameter of 1 μm prepared from an Yttrium Iron Garnet (YIG) film with the thickness 52 nm grown by liquid phase epitaxy on a GGG (111) substrate. The parameters of the disks were determined within WP1 using the MRFM technique (see D1.2). These measurements yielded the saturation magnetization $\mu_0 M_s = 176$ mT and the Gilbert damping parameter $\alpha = 1.6 \times 10^{-3}$. In our studies, the excitation of the magnetization dynamics is performed by using an Au microwave transmission line with the width of 8 μm and the thickness of 200 nm (Fig. 1) that creates a dynamic field *h* nearly uniform across the disk area. Two microwave-frequency sources are connected to the antenna via a power combiner and are applied simultaneously in 1-μs pulses (unless specified otherwise). The static magnetic field H_0 is applied at a 45° angle to allow the efficient excitation of spin waves both with direct-excitation and parametric-pumping mechanisms. H_0 is set at 15 mT and 30 mT, depending on the studied non-linear regime.

We focus the probing laser light with the wavelength of 473 nm and the power of 0.25 mW into a sub-

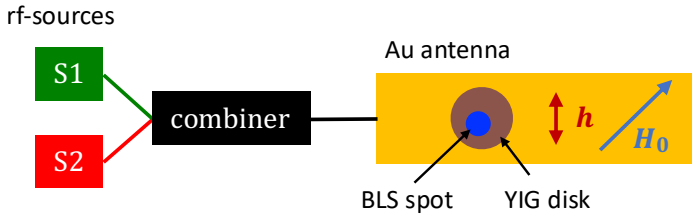

Figure 2: Schematics of the experiment. Two rf-sources provide an rf-current to the wide antenna patterned on top of the 1-μm disk. The static magnetic field H_0 is oriented at 45° with respect to the microwave field h of the antenna, allowing both transverse and parametric excitation of the magnetization dynamics. The magnetization oscillations are measured using μ-BLS.

micrometer diffraction-limited spot on the surface of the YIG disk (Fig. 1) and analyze the modulation of the probing light by the magnetization oscillations using a high-contrast optical spectrometer. The obtained signal – the BLS intensity – is proportional to the intensity of magnetic oscillations at a given frequency, i.e. to the magnon population in each mode.

1.2 Observation of spontaneous scattering

Figure 3 shows the spin-wave amplitude (square root of the BLS intensity) as a function of the frequency of the primary excitation source S1 (f_1 from 1.8 to 2.4 GHz with a 5 MHz spacing on the y-axis) for 6 different powers: 2.5, 10, 20, 100, 200 and 300 mW.

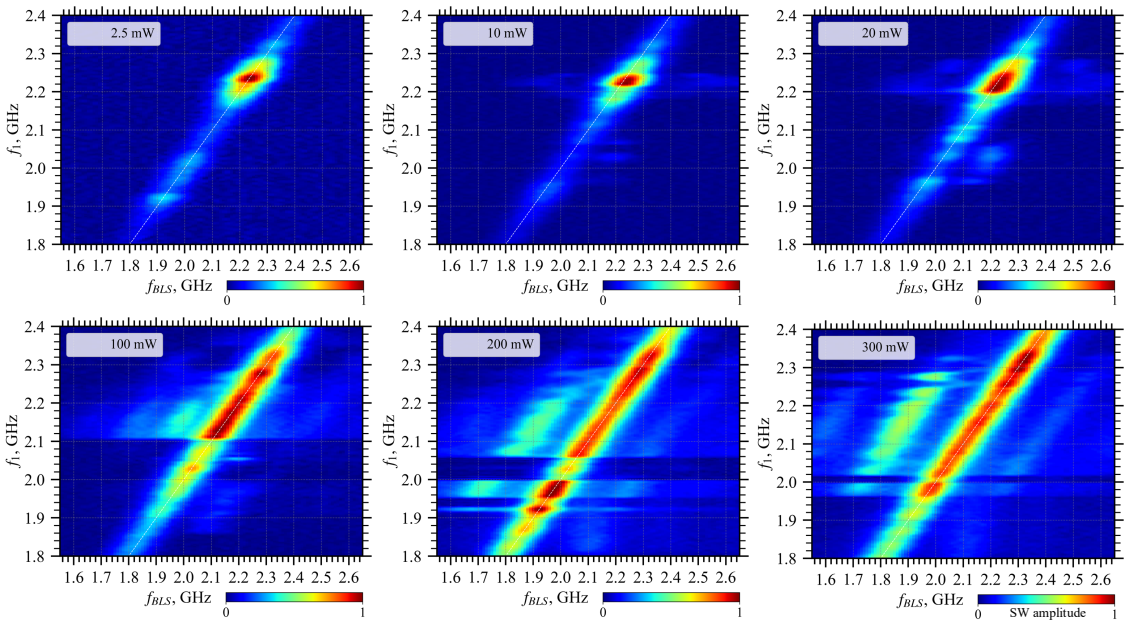

Figure 3: Color maps of the SW amplitude obtained from the BLS spectra as a function of the applied frequency f_1 (y-axis) at different applied powers $P_1 = 2.5, 10, 20, 100, 200$ and $300\ mW$. At low power, only a resonance at f_1 is detected (white dotted line). At increased powers, the magnon scatter from the resonant mode to other modes.

At low power ($P_1 = 2.5$ mW), the system is in the linear regime and the spin waves are excited only at the frequency of excitation. The fundamental mode is excited around 2.24 GHz at an applied field $H_0 = 30$ mT. From simulation and our previous experiments with parametric pumping, we know that bulk modes of the 1-µm disk are located within less than 100 MHz or above the fundamental mode. Thus, we identify the bright spots around 1.9 - 2.0 GHz as corresponding to different edge modes.

When the power is increased to 10 and 20 mW, off-diagonal spots appear on the maps. This indicates that magnons can scatter from the excited mode to other discrete modes. As the power is increased, the resonance of the fundamental mode forms a wide plateau as it shifts down in frequency. Under these conditions, an efficient scattering is observed to frequencies given by:

$$f_{scatter}^{n} = f_1 - n * \Delta f_0$$

Where Δf_0 is of the order of hundreds of MHz and depends on the applied power. The spectrum appears to be no longer discrete but is rather continuous and dominated by the non-linear behavior of the fundamental mode.

In this regime highly non-linear regime, we first analyze the properties of the spontaneously created scattering peaks, i.e. what synaptic weights are created and how they can be controlled. In a second part, we show that applying a second rf-source allows to control the scattering, greatly increasing its efficiency through a nonlinear stimulation process.

2 SPONTANEOUS AND STIMULATED SCATTERING IN THE DEEP NON-LINEAR REGIME

In this part, we focus on the nonlinear scattering at microwave powers P_1 between 50 mW and 360 mW for the cases of a single rf source (spontaneous scattering) and two sources (spontaneous and stimulated scattering).

2.1 Spontaneous scattering

Thanks to the spectral resolution of the BLS setup, we have access to the spectral components generated in the non-linear regime. The normalized spin-wave spectrum is plotted for an excitation frequency $f_1 = 2.175$ GHz for different applied powers in Figure 4 (a). At $P_1 = 100$ mW (blue curve), we observe clear scattering at evenly spaced peaks whose frequencies are such that:

$$f_{scatter}^{n} = f_1 - n * \Delta f_0$$

with $\Delta f_0 \approx 150$ MHz. The first-order peak ($n = 1$) has the largest amplitude, almost half as large as that of the resonance peak. When the power is increased, the spacing Δf_0 between each scattering order increases as well as the amplitude of the peaks at all orders. The spectra measured at different powers are aggregated on a color map in Figure 4 (b). It clearly shows the evolution of the position and intensity of the scattering peaks at all orders.

We can also notice a scattering at a frequency larger than f_1. This frequency does not significantly change with increasing power.

The characteristics of the main scattering peak at $f_{scatter} = f_1 - \Delta f_0$ are extracted and shown in Figure 5 (a). The frequency spacing Δf depends logarithmically on the applied power and is doubled between 20 dBm and 25.5 dBm, reaching nearly 300 MHz.

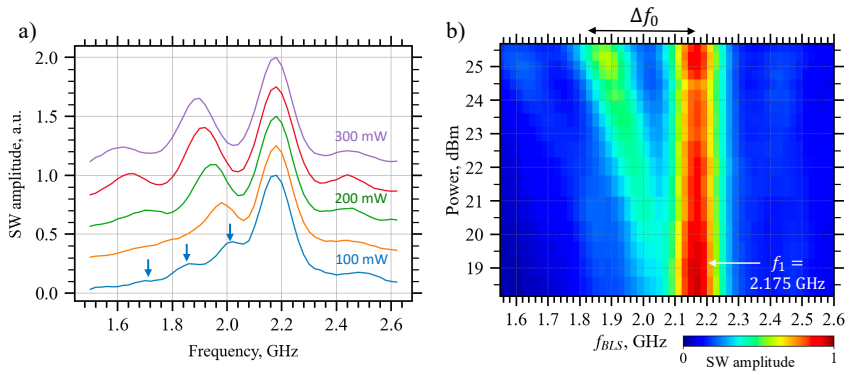

Figure 4: Spin-wave amplitudes for an applied frequency $f_1 = 2.175\ GHz$ and a power $P_1 = 100, 150, 200, 250, 300\ mW$ (a). Spontaneous scattering at multiple orders is marked with the blue arrows. It is possible to follow the position and intensity of the scattering peaks as a function of applied power P_1 on a color map (b). The splitting Δf_0 increases with P_1.

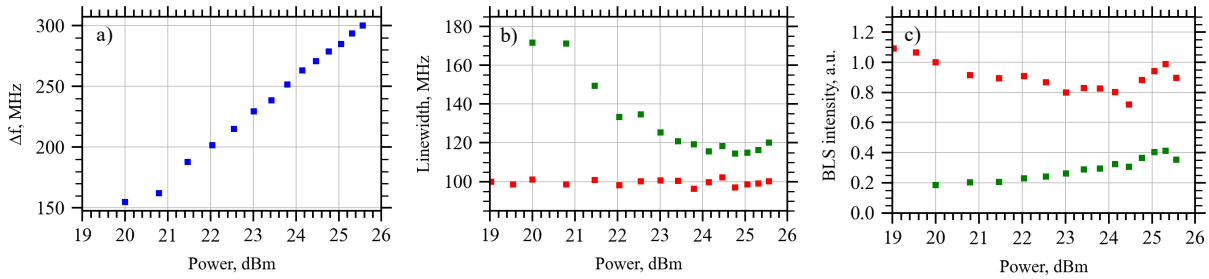

Figure 5: Characteristics of the first scattering peak. (a) The frequency splitting with the primary peak Δf_0 increases logarithmically with the applied power. The linewidth of the scattering peak decreases and its intensity increases with power (green squares in b,c) while the linewidth of the primary peak and its intensity remain almost constant (red squares)

In that span, the linewidth of the secondary peak is reduced from 180 to nearly 110 MHz, while the linewidth of the primary peak is independent of the applied power (Figure 5 b). Increasing the power leads to an increase of the lifetime of the scattered magnons until a certain point (around 25 dBm). This is directly linked to an increase of the scattering efficiency, as shown on Figure 5 (c). While the main peak intensity decreases by about 10-20% with the increase in power, the intensity in the scattered mode is more than doubled between 20 and 25 dBm, despite the increase in Δf. Both effects saturate around 25 dBm.

We stress that the linewidth shown here is altered by the instrumental linewidth of the BLS setup. To correctly measure the magnons lifetime, we use either a secondary low-power probe or a time-resolved measurement of the rising and falling edges.

There are two alternative ways to interpret the observed scattering, either in the time or in the frequency domain. In the time domain, the large intensity of the fundamental mode can locally change the internal magnetic field, which in turn changes the profile of the mode and results in additional changes of the internal magnetic field. This self-action process can be unstable and can lead to a temporal modulation of the spin-wave envelope that can be periodic or even chaotic. This process is usually referred to as dynamic instabilities, modulation instabilities or self-modulation. In particular, it was studied within the consortium at the CEA using MRFM on an out-of-plane magnetized Bi-YIG disks with perpendicular uniaxial anisotropy. It was demonstrated that the negative non-linear frequency shift leads to an early saturation of the precession angle and thus a plateauing of the resonance due to dynamic instabilities. On the contrary, in the in-plane magnetized disks with positive non-linear frequency shift, the self-interaction of the mode with the internal field is stable and large precession angles can be reached. Similarly, when we performed our experiments for the out-of-plane field configuration (positive non-linear frequency shift), no scattering was observed. Instead, we observed a well-defined foldover-like resonances. Although the μ-BLS has the time resolution to study such phenomena, these instabilities occur with a random phase. Thus, even single sweep of the BLS only gives the magnetization oscillations averaged over many repetitions of the dynamic instability.

Nevertheless, the μ-BLS provides direct access to the frequency-domain picture of this phenomenon. When the fundamental mode f_1 is excited above a certain threshold amplitude, its energy is redistributed via four magnon scattering within the magnon bands. As frequency $f_1/2$ falls within the magnon gap (no available modes), three-magnon scattering processes are absent in the disk at the used frequencies. Thus, the leading non-linear mechanism is the four-magnon scattering. In this process, the annihilation of two

magnons at f_1, leads the creation of a first pair of magnons (f_+, f_-) under conservation of energy and momentum. These magnons can themselves scatter with a magnon at f_1, creating a cascade of scattering at different orders such that:

$$f_{\pm}^{n} = f_1 \pm n * \Delta f_0$$

We note that in the experiment, most modes f_+^n are not resolved. This could be due to the strong decrease of the BLS sensitivity for large k-vectors. Furthermore, it is not guaranteed that the scattering is resonant. Indeed, in the case of a microscopic disk with discretized spectrum, there might not be modes available at scattering frequencies and non-resonant scattering might dominate.

2.2 Frequency combs at high power

First, we study the case where both sources have large power: $P_1 = P_2 = 100\ \mathrm{mW}$. As shown in Figure 3, sweeping a single source at this power yields an efficient scattering of magnons to $f_{scatter} = f_1 - n * \Delta f_0$, where Δf_0 is independent of the applied frequency. Therefore, in this experiment, we define the frequencies f_1 and f_2 in the following way:

i. The frequency spacing Δf is kept constant and only the central frequency f_c is swept from 1.8 to 2.4 GHz.

$$f_1 - f_2 = \Delta f$$

ii. Each sweep is repeated for different values of Δf, from 0 to 600 MHz.

Both signals are applied simultaneously using a 500-ns pulses with 2-µs repetition period.

The measurement of each sweep can then be represented on a color plot as shown in Figures 6 (a,b,c,d) for different values of Δf.

For a large frequency spacing $\Delta f = 500\ \mathrm{MHz}$, both resonances do not significantly interact with each other (Figure 6 (a)). The spectrum is simply the sum of the responses generated by each source. The spontaneous scattering due to each source is visible (note that the color maps represent the SW intensity here).

As the frequency spacing between f_1 and f_2 is reduced, both responses start to interact. In particular, we observe that for a certain range of Δf ($\sim$ 120 MHz to 240 MHz), the magnons scatter to evenly spaced modes whose spacing in frequency is equal to Δf. The scattering can be particularly efficient, with high intensity of the scattered mode, up to the 4th order for $\Delta f = 140\ \mathrm{MHz}$ (figure 6 (b)). We also note that the stimulated scattering occurs in a much wider frequency range ($\sim$300 MHz, see Figures 6 (b,c,d)) in comparison to the spontaneous scattering in the case of single-source excitation ($\sim$100 MHz, see Figure 6 (a)).

This phenomenon can be considered as stimulated four-magnon scattering. The presence of the secondary excitation, used as a seed mode, results in well-defined frequency combs whose spacing is controlled by the frequency difference between the seed and the primary mode.

To get a more precise picture of the stimulated scattering, the spectrum for a microwave power $P_1 = P_2 = 100\ \mathrm{mW}$, $f_1 = 2.18\ \mathrm{GHz}$ and $\Delta f = 170\ \mathrm{MHz} \approx \Delta f_0$ is plotted in Figure 7 (black curve). The individual response for sources applied separately are given in green (S1) and red (S2). As previously observed, the intensity of the scattering modes is strongly enhanced. The linewidth of the scattering modes is also reduced, indicating that the scattering increases the lifetime of those modes.

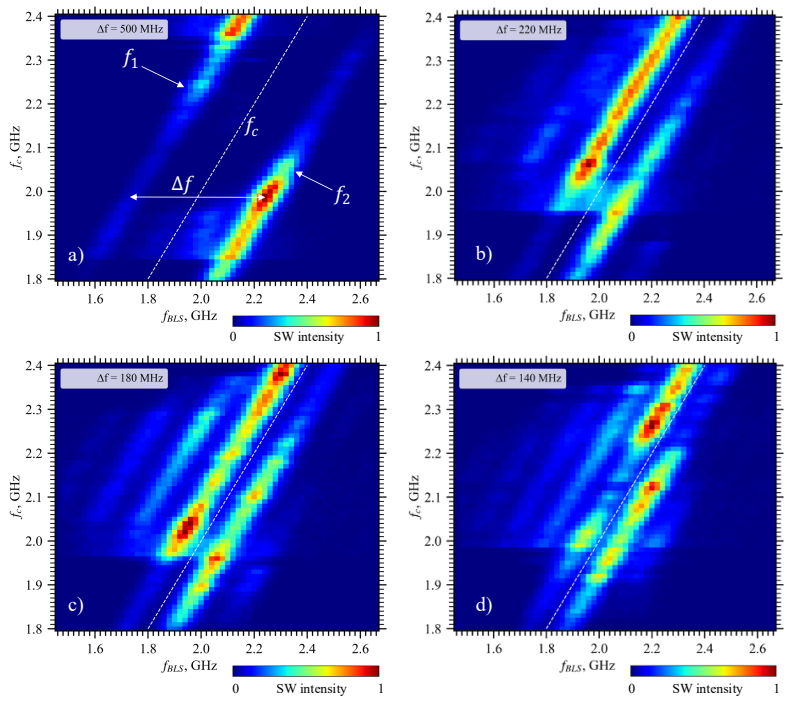

Figure 6: Color maps of the aggregated BLS spectra measured for different excitation frequencies f_1 and f_2. Each map corresponds to a given spacing $\Delta f = f_2 - f_1$. In each map, Δf is kept constant and the central frequency $f_c = (f_1 + f_2)/2$ is swept (indicated on the y-axis).

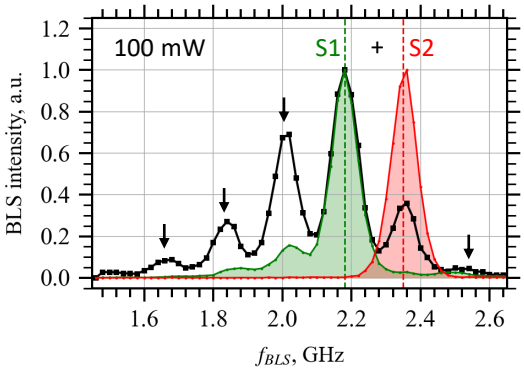

Figure 7: Normalized BLS spectrum showing the stimulated scattering at P=100 mW, $f_1 = 2.18\ GHz, f_2 = 2.35\ GHz, \Delta f = 170\ MHz$ (black curve). The BLS spectra corresponding to the application of the sources separately are shown in green (S1) and red (S2). The intensity of the scattering peaks is strongly enhanced at all orders (black arrows) and their linewidth is reduced.

Similar results were obtained at larger power ($P = 200$ mW), with the frequency comb extending over the whole range of f_c and an increased range of Δf up to 300 MHz instead of 240 MHz.

3 CONCLUSION AND OUTLOOK

Our results demonstrate that by applying a direct high-power excitation we can put the magnetic system into a deep non-linear regime characterized by an efficient transfer of energy among multiple spin-wave modes. This direct transfer of energy emerges by dynamic self-modulation of the internal field and can be described as a four-magnon scattering process.

By adding a second excitation source, the strength of the scattering, i.e. the synaptic weights can be effectively controlled by varying the frequency and power of the second RF source. This corresponds to the k-NN schematically represented in Figure 8 (a).

The secondary excitations can be a direct excitation (as shown in this report) or a parametric excitation (as shown in D2.1). This gives us extra flexibility to program our k-neural network, as an intermediate mode can be addressed with a sub-threshold parametric excitation and create or control another synapse.

The complexity of the k-NN can be further increased using an arbitrary signal generator that will be able to address simultaneously and independently a large number of input and programming signals. This will be implemented in our future experiments. In these experiments, we expect to clarify the nature of the interaction between the sets of modes in multiple frequency combs (Fig. 8 b).

Finally, as scattering at higher order originate from a temporal cascading effect, we expect that a control of the pulse timing can also effectively control the individual synaptic weights. This is the subject of new investigations as part of the task 2.3 on advanced programming methods.

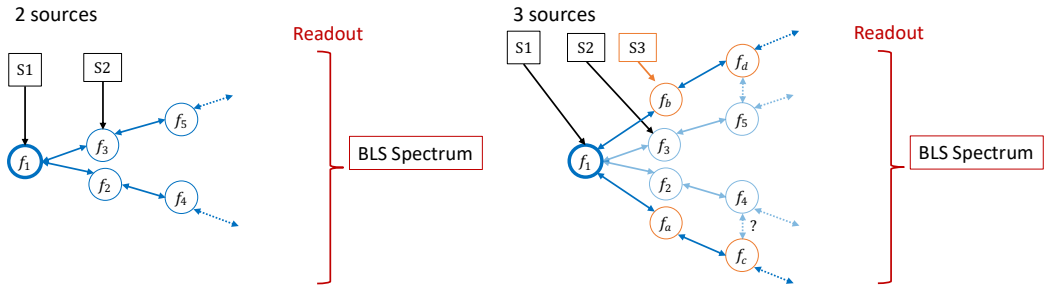

Figure 8: Schematic of the k-NN implemented in the experiment with 2 sources and its possible extension by using 3 sources.

The experimental studies have recently started on the 2nd generation of samples using the experimental methodology developed with the 1st sample. First tests have shown that the new samples possess a mode structure, which is much closer to the theoretical expectations, and a three times lower Gilbert damping in comparison to the previous samples. As a results, the thresholds of three- and four-magnon scattering processes are significantly lower, and very encouraging results can be obtained using non-resonant three-magnon scattering. Furthermore, the new sample contains high-quality structures with many different sizes of disks and ellipses that will be used to determine the optimum spectrum of spin-wave modes and identify the most favorable conditions for their nonlinear interactions. For instance, high-quality sub-micrometer-size YIG disks show a strong frequency splitting between the modes, which will greatly increase our ability to individually detect them and to quantitatively characterize their nonlinear interactions.

These findings are being used to support the implementation of a simulation based k-space learning algorithms to build complexe k-NN protocols that will be implemented experimentally.